

NASA TECHNICAL NOTE



NASA TN D-3537

c. 1

NASA TN D-3537

LOAN COPY: 1
AFWL (M)
KIRTLAND AF



COMPRESSED-AIR MODEL INVESTIGATION
OF SOLID ROCKET OVERPRESSURES
DUE TO INTERFERENCE FROM
AFT-END IGNITION ROCKET

by Reino J. Salmi

*Lewis Research Center
Cleveland, Ohio*



TECH LIBRARY KAFB, NM



0130288

NASA TN D-3537

COMPRESSED-AIR MODEL INVESTIGATION OF SOLID ROCKET
OVERPRESSURES DUE TO INTERFERENCE FROM
AFT-END IGNITION ROCKET

By Reino J. Salmi

Lewis Research Center
Cleveland, Ohio

NATIONAL AERONAUTICS AND SPACE ADMINISTRATION

For sale by the Clearinghouse for Federal Scientific and Technical Information
Springfield, Virginia 22151 - Price \$1.00

COMPRESSED-AIR MODEL INVESTIGATION OF SOLID ROCKET OVERPRESSURES DUE TO INTERFERENCE FROM AFT-END IGNITION ROCKET

by Reino J. Salmi

Lewis Research Center

SUMMARY

An experimental investigation was made to determine the effects on the combustion chamber pressure of a large, solid-propellant, booster rocket due to an aft-end ignition rocket firing into the booster grain port through the exhaust nozzle. The tests were made with 1/14.2 scale models that simulated those used in the current 260-inch solid rocket program. Additional ignition-rocket models were used to study the effects of various parameters. The rocket exhaust gases were simulated with compressed air.

The results indicated that the igniter interference could cause large overpressures in the booster-rocket combustion chamber. The magnitude of the interference effect due to the ignition rocket was dependent on the ignition-rocket position, diameter, pressure ratio, and weight flow. At low igniter-to-booster chamber-pressure ratios, which correspond to the condition where the booster rocket is at its design chamber pressure, the interference effect varied greatly with igniter position. Increases in the booster chamber pressure to 60 percent, depending on ignition-rocket geometry, occurred when the igniter was 0.2 of the booster throat diameter downstream of the nozzle throat. At a station corresponding to 0.6 diameter, the interference effects were generally negligible. At high igniter-to-booster pressure ratios, which reflect the low booster chamber pressures at the initial ignition phase, the booster chamber pressure was greatly increased by the igniter jet, as would be desired for rapid ignition; however, the position of the ignition rocket in the booster nozzle had little effect.

INTRODUCTION

A current method of igniting large, solid-propellant, booster rockets, such as the 260-inch solid rocket, uses the exhaust gases of a small high-pressure solid rocket for the ignition energy. In this technique, the ignition rocket is located in the exhaust nozzle

of the booster rocket and is fired forward directly into the large grain port. The booster propellant is ignited by the heat received from the igniter exhaust gases, and the ignition is augmented by the increase in pressure produced by the igniter exhaust flow. When the ignition has proceeded to an acceptable point, as indicated by the chamber-pressure rise, the ignition rocket is ejected to prevent any perturbations to a normal pressure buildup in the booster.

Some experiments with small, solid rockets (ref. 1) were made to determine the interference effects on the booster rocket in the event that the ignition rocket was not ejected because of failure of the release mechanism. The results indicated that overpressures high enough to cause failure of the booster-rocket casing could occur.

A condition could also exist where it would not be convenient to remove the ignition rocket. For example, when the booster rocket is launched from the earth, the ignition rocket will be located on the launch pad below the booster. In this case, a fixed ignition-rocket position that provided good booster ignition and that had a negligible effect on the design chamber pressure would be desirable.

In order to define the severity of the interference problem, and to determine the major parameters influencing it, an experimental investigation was conducted at the Lewis Research Center by using 1/14, 2 scale models with compressed air to simulate the exhaust gases. The geometry of the models was tailored to provide information applicable to the current 260-inch solid rocket program. Additional ignition-rocket models were made, however, to determine the effects of ignition-rocket size and mass flow rate.

The investigation was conducted in the Propulsion Systems Laboratory altitude test facility that permitted the use of relatively large models without excessive air flows and pressures to obtain the desired range of igniter-to-booster pressure ratios. Steady-state data were obtained for various booster combustion chamber pressures and ignition-rocket positions with the simulated ignition jet both off and on.

Results are presented that show the effects on the booster rocket chamber pressure resulting from the ignition-rocket position, igniter-to-booster total-pressure ratio and ignition-rocket mass flow. Diagrams indicative of the flow phenomenon in the booster nozzle are also presented.

SYMBOLS

- A area, sq in.
- A^* throat area, sq in.
- A_1 annular area between booster nozzle and ignition rocket

D	diameter, in.
D^*	throat diameter, in.
P_c	booster combustion chamber pressure, psia
ΔP_c	$P_c - P_{c,0}$, psi
$P_{c,0}$	initial booster-rocket combustion chamber pressure when not influenced by ignition rocket, psia
P_i	ignition rocket total pressure, psia
X	distance from booster nozzle throat plane measured parallel to model center-line, in.
X_i	distance from booster nozzle throat plane to ignition rocket model, in.
ϵ	geometric area ratio parameter, ratio of minimum annular flow area between ignition rocket and booster nozzle to booster throat area (fig. 13), A_1/A_b^*
ϵ_e	ratio of effective throat area based on experimental results to booster throat area
γ	ratio of specific heats
θ	nozzle half-angle, deg

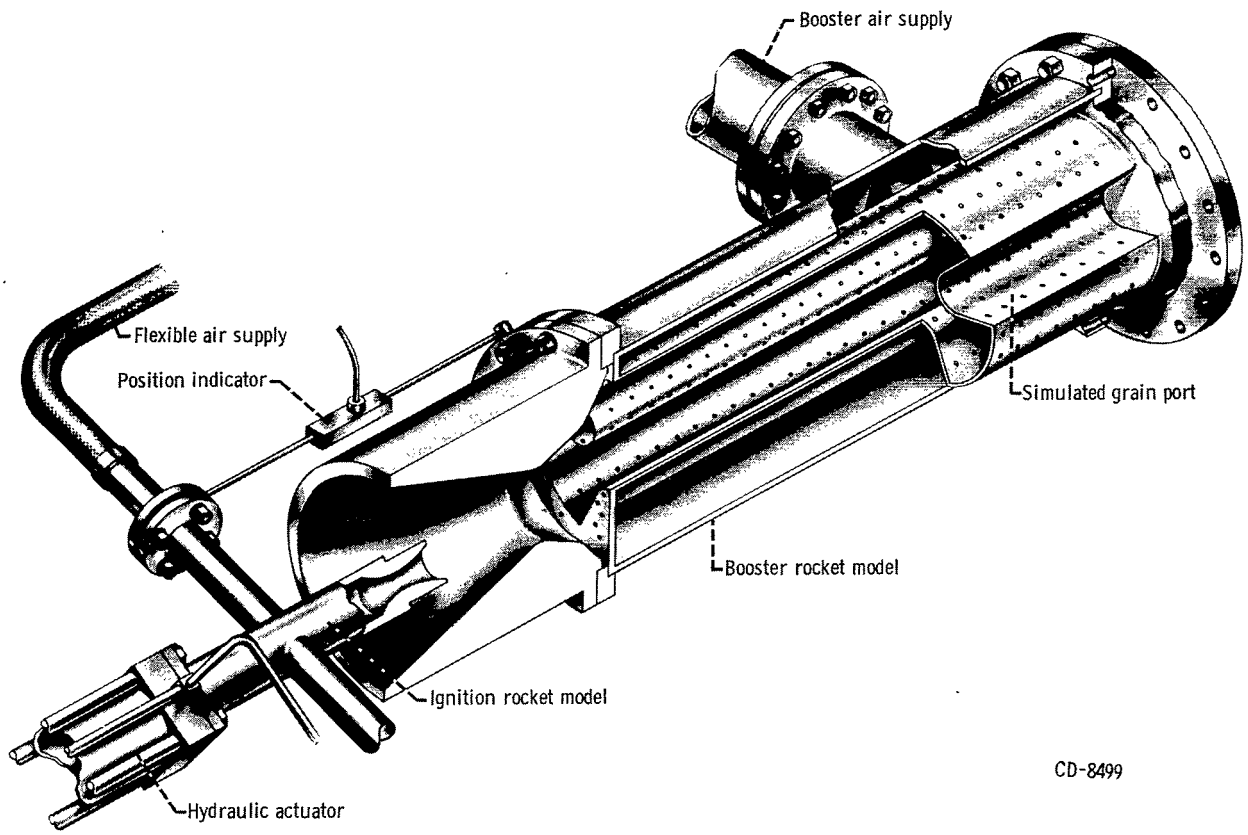
Subscripts:

b	booster model
e	effective
i	ignition rocket
n	nozzle exit

APPARATUS

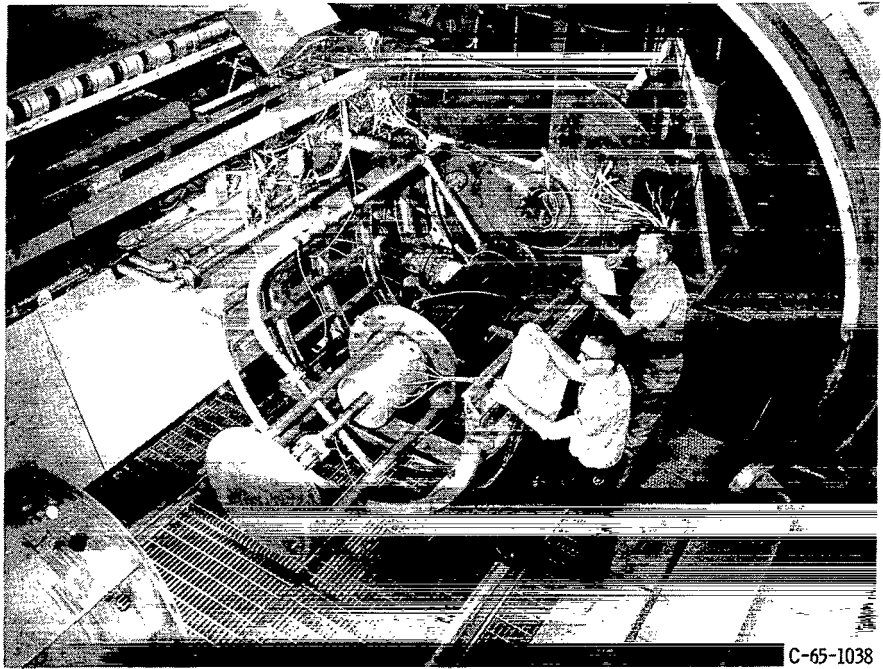
Models (1/14.2 scale) of the Aerojet General 260-inch solid rocket and its ignition rocket along with four additional ignition-rocket models of varying geometry were fabricated to be used with compressed air. The models were mounted for testing, as shown in the schematic diagram in figure 1. A photograph of the models in the test facility is presented in figure 2. The geometry and dimensions of the booster and igniter-rocket models are given in figures 3 and 4. The geometry of igniter-rocket model 1 corresponds to that of the igniter used in the first firing of the 260-inch solid rocket.

To simulate the effect of gas generation from the burning booster propellant grain, the inner surface of the booster grain was simulated by using perforated steel. The perforated area was about 65 percent of the booster-nozzle throat area. A photograph of



CD-8499

Figure 1. - Schematic diagram of test setup.



C-65-1038

Figure 2. - Test facility and model setup.

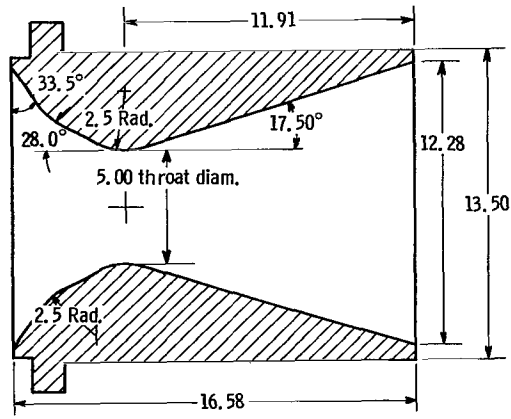
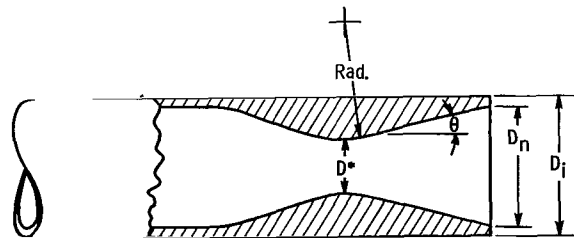
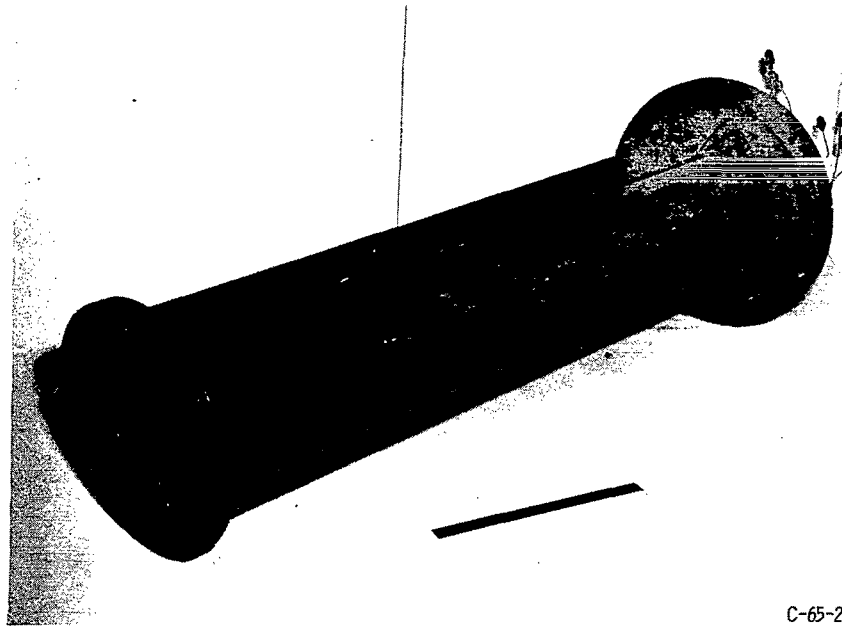


Figure 3. - Geometry of booster nozzle. (All dimensions are in inches except as noted.)



Model	Ignition rocket diameter, D_i , in.	Throat diameter, D^* , in.	Nozzle exit diameter, D_n	Radius, Rad, in.	Nozzle half angle, θ , deg	Nozzle area ratio, A_n/A^*
1	2.11	1.02	2.11	2.04	15.0	4.28
2	2.85	1.02	2.11	2.04	15.0	4.28
3	2.53	1.21	2.52	2.42	15.0	4.33
4	2.85	1.21	2.52	2.42	15.0	4.33
5	2.85	1.51	2.84	3.02	15.0	3.54

Figure 4. - Geometry of ignition rocket models.



C-65-2649

Figure 5. - Booster rocket simulated grain core.

the simulated grain is presented in figure 5.

The igniter model was mounted in the test setup so that its centerline was common with that of the booster model. The location of the igniter-rocket model relative to the booster rocket was varied by a hydraulic actuator attached to a rigid framework extending from the booster-rocket model, as shown in figure 2. A linear potentiometer indicated the position of the igniter rocket relative to the booster model.

Compressed air was supplied to the booster rocket model by a 6-inch pipe to the annular area surrounding the simulated grain core and to the ignition-rocket model by a smaller flexible hose to allow axial movement of the model. The pressures were measured with strain-gage-type transducers and recorded on multichannel oscillographs. The air temperatures were measured with thermocouples and read from potentiometers. Standard orifices were used to measure the air flow rates.

PROCEDURE

The tests were performed in the Lewis Propulsion Systems Laboratory altitude chamber 2. The range of igniter-to-booster chamber-pressure ratios simulated that of the 260-inch solid rocket for booster-chamber pressures varying from the initial atmospheric pressure to about 25 percent above the design chamber pressure. To obtain the desired pressure ratios with a limited air supply and maximum size models, the ambient pressure in the test cell was set at 1.17 pounds per square inch absolute.

The general test procedure was to set the booster chamber pressure at various fixed values with the ignition rocket withdrawn from the booster nozzle. The ignition rocket, with its jet off, was then moved forward into the booster nozzle to the most rearward position, and steady-state data points were taken with the ignition jet initially off, and then with the ignition jet on. This procedure was repeated for more forward positions of the ignition rocket. For a given chamber-pressure setting, the booster mass flow remained constant because of the choked flow through the simulated grain port. To simulate the conditions prior to booster grain ignition, data were also obtained with air flow only to the ignition rocket.

RESULTS AND DISCUSSION

Application of the results of the present investigation to the actual solid rocket problem requires consideration of the differences between the actual case and the model tests. The main factors to be considered are the Reynolds number, or scale effect, and

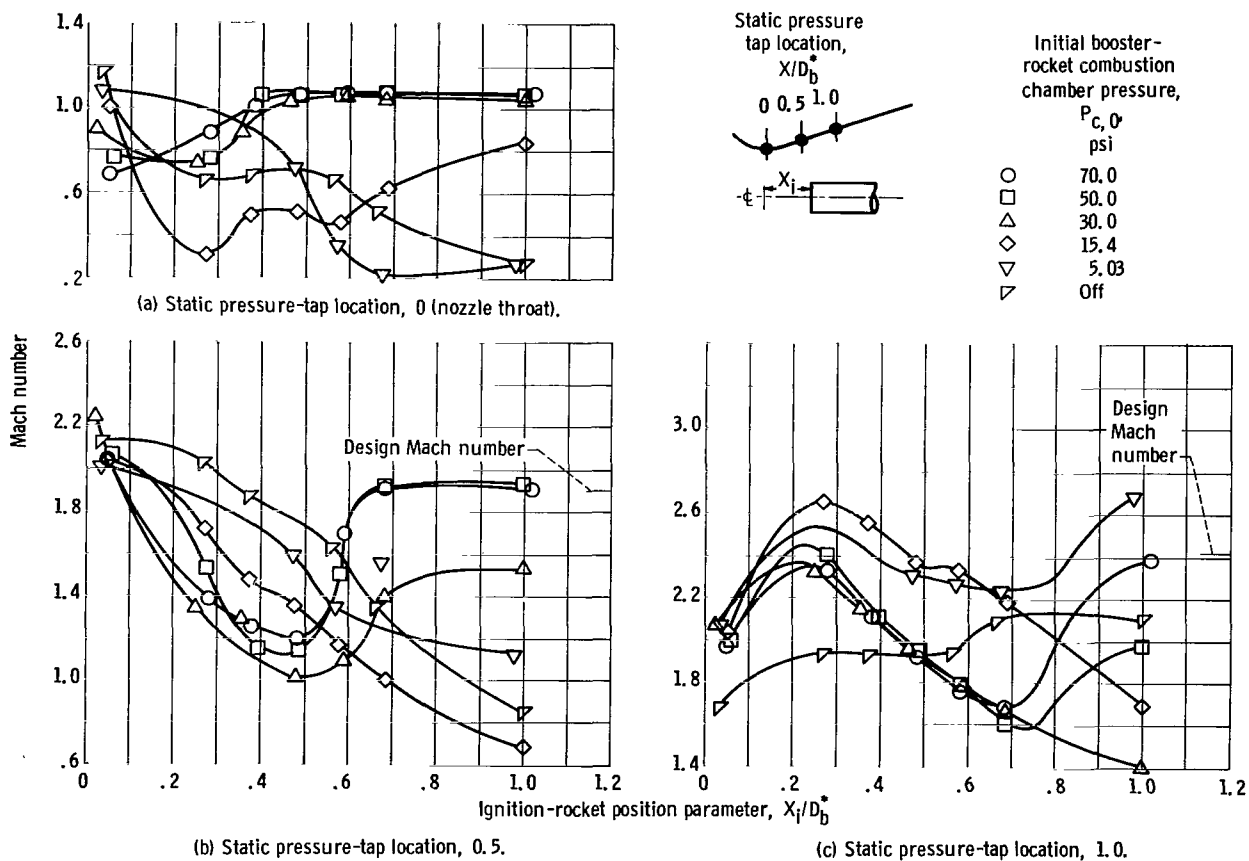


Figure 6. - Effect of ignition-rocket position on booster-nozzle-wall Mach number for various initial booster chamber pressures. Ignition rocket total pressure, 92 pounds per square inch absolute. Ignition-rocket model 1.

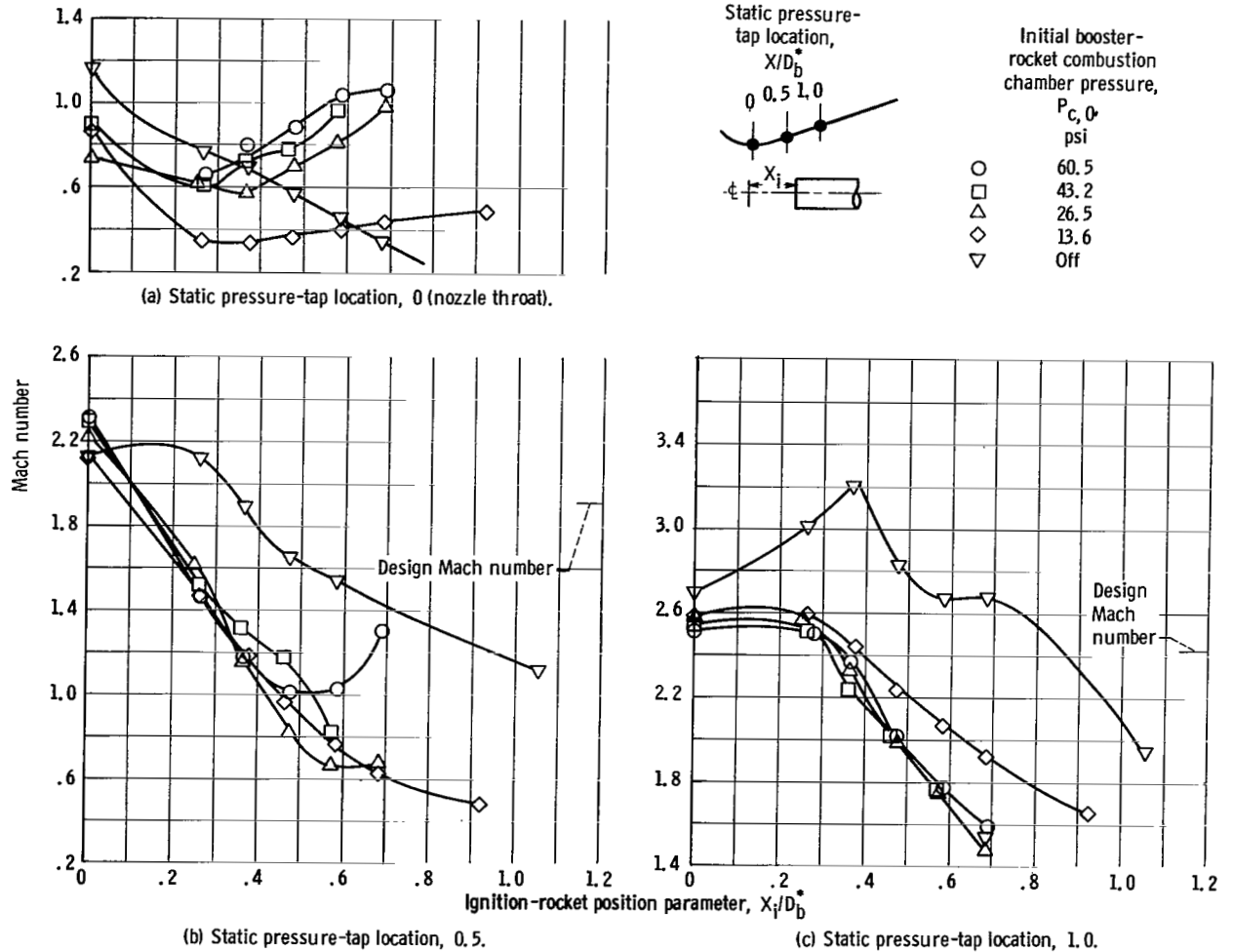


Figure 7. - Effect of ignition-rocket position on booster-nozzle-wall Mach number for various initial booster chamber pressures. Ignition-rocket total pressure, 79 pounds per square inch absolute. Ignition-rocket model 5.

the differences in the exhaust gases, which consist of air for the model and high-temperature combustion products for the actual rocket.

The primary difference that occurs in considering the exhaust products is the effective value for the ratio of specific heats γ . In the model tests, the effective value of γ is 1.4, whereas for the solid rocket, γ is approximately 1.2. A compensating factor, however, is the fact that in each case, the values of γ for the booster rocket and the ignition rocket are approximately equal. From a comparison of the normal shock pressure recovery and the static-to-total pressure ratios as a function of flow area ratio for $\gamma = 1.2$ and $\gamma = 1.4$, the effects of γ on the flow patterns appeared to be small. The relative weight flows from the booster and the igniter will, in each case, depend primarily on the relative throat areas and combustion chamber pressures.

The Reynolds number effect could be more significant, however, since there is a difference of about an order of magnitude in size from the model to the full-scale booster.

However, for the present model, the Reynolds number based on the booster nozzle-throat diameter was about 6.5×10^6 for the on-design chamber-pressure condition. This Reynolds number is relatively high, and it is believed that the influence of even much higher Reynolds numbers would affect the geometry of the flow patterns only slightly. Therefore, it is concluded that the overall differences between the present results and those for the actual case are of second order.

Another factor that does not affect the validity of the results but which should be kept in mind when applying them to the actual case is the difference between the present steady-state conditions with air and the actual conditions for a burning propellant grain with an increasing chamber pressure. The propellant-grain burning rate and, hence, the exhaust-gas generation rate, generally, increases with increasing combustion chamber pressure. Therefore, any increase in the normal chamber pressure caused by interference effects of the ignition rocket will also increase the burning rate, and an additional increase in the chamber pressure will result. This phenomenon does not occur, of course, in the situation where the exhaust gases are air.

To understand and discuss the interference phenomenon that produces the booster overpressures, it is desirable to provide a model of the booster and ignition-rocket flow patterns. In the present case, actual observations were not feasible, but approximate flow patterns could be constructed from measurements indicative of the booster-nozzle Mach number. For various booster combustion chamber pressures, Mach numbers based on the nozzle-wall static pressure and combustion-chamber total pressure are shown as functions of ignition-rocket position in figures 6 and 7 for models 1 and 5, respectively. Model 1 represents the smallest ignition rocket with minimum weight flow, and model 5, the largest ignition rocket with maximum weight flow. The results should therefore bracket the other cases. Flow models that outline the boundary or interface between the ignition-rocket exhaust flow and the exhaust flow from the booster rocket were constructed for values of the ignition-rocket position parameter X_1/D_b^* of 0.37 and 0.60 and are shown in figures 8 and 9. The flow boundaries were constructed by using the area ratios at each nozzle station corresponding to the local Mach number. These flow boundaries indicate two types of flow conditions in which the igniter jet either penetrated the booster grain port or was turned back in the booster exhaust nozzle. In general, the igniter flow penetrated the booster grain port only at relatively low booster chamber pressures.

The more general flow pattern occurs when the ignition-rocket jet is turned back in the booster exhaust nozzle. The diagrams of figure 10 show, schematically, two basic types of flow for this case. Figure 10(a) presents the case where no interference effects are felt in the booster combustion chamber as a result of the igniter jet. Here, the booster nozzle flow is sonic at its physical throat, expands supersonically in the nozzle, and forms a bow wave ahead of the ignition-rocket jet. This flow pattern is typical of

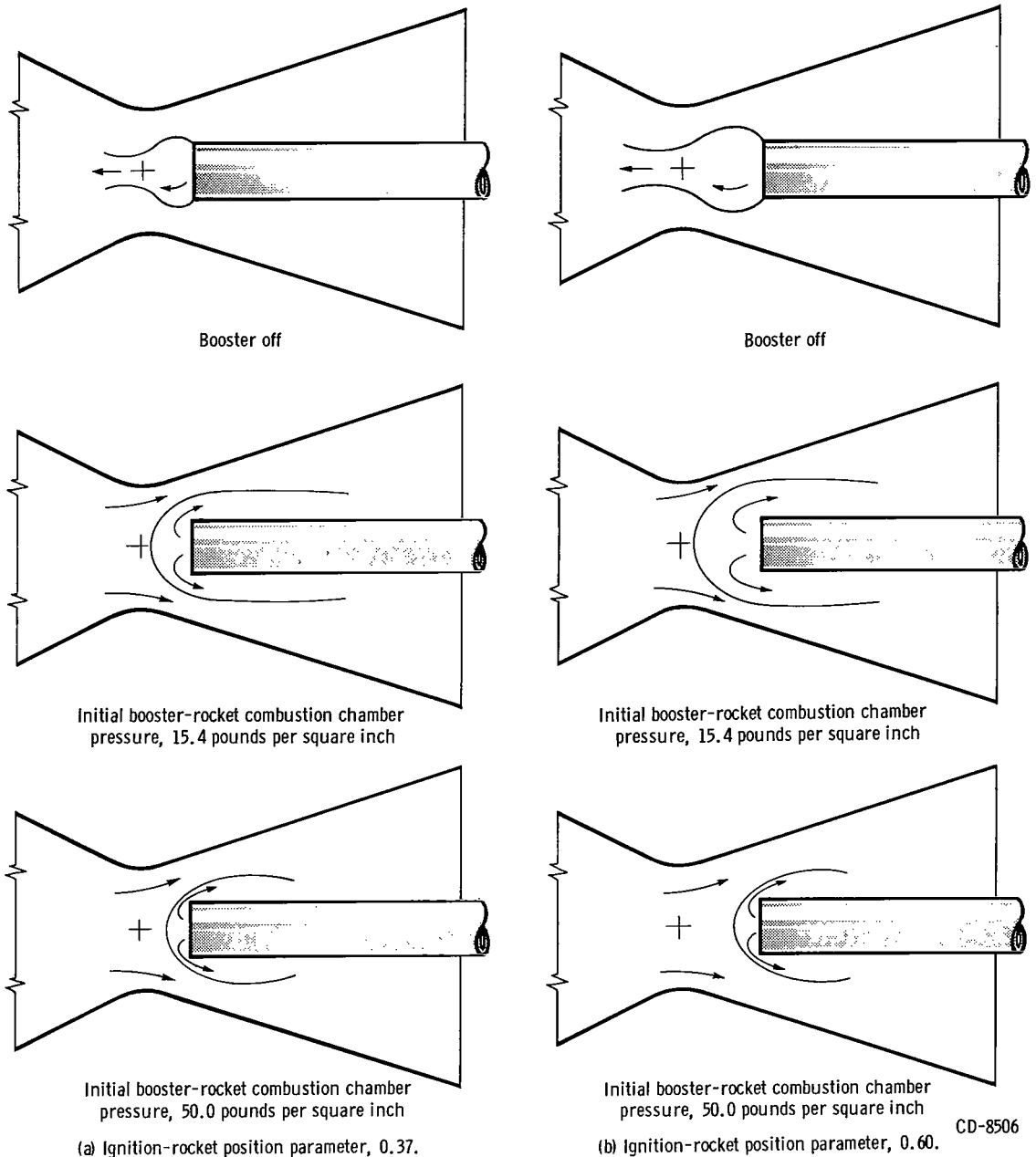


Figure 8. - Ignition-jet-flow boundaries constructed from nozzle Mach number distributions. Ignition-rocket total pressure, 92 pounds per square inch absolute. Ignition-rocket model 1.

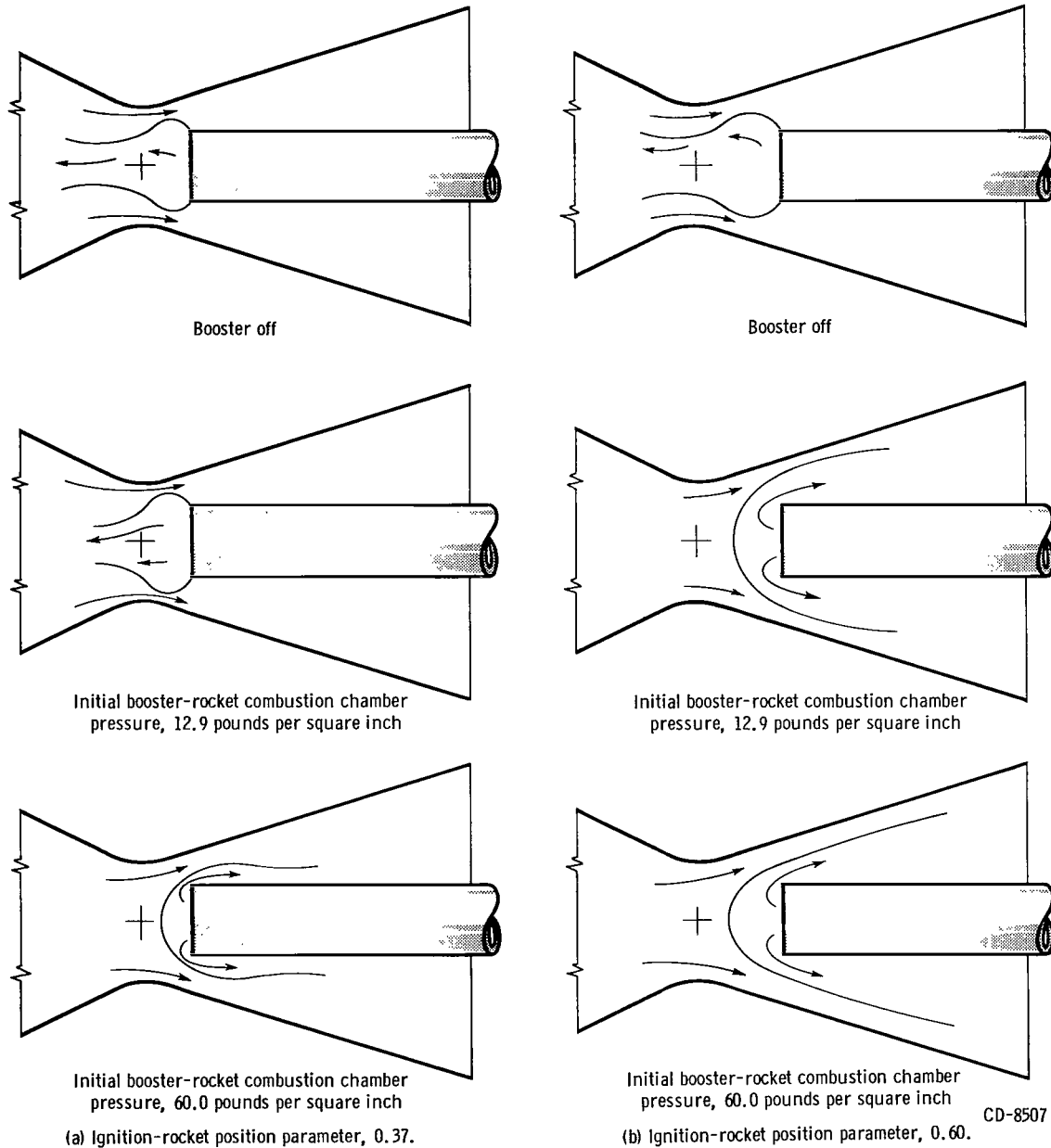
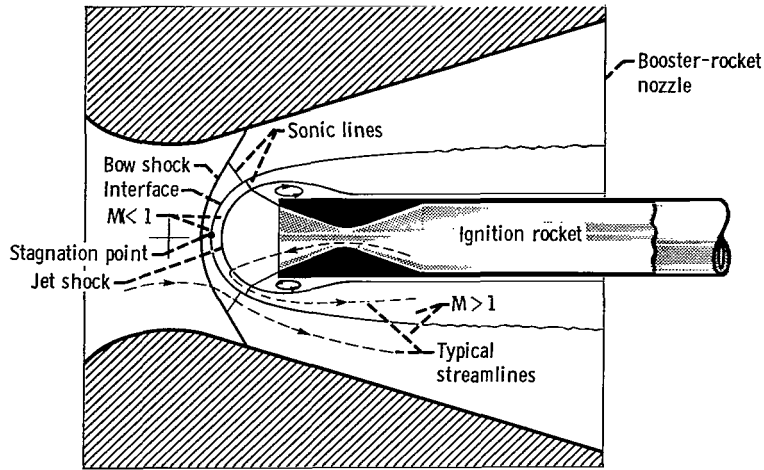
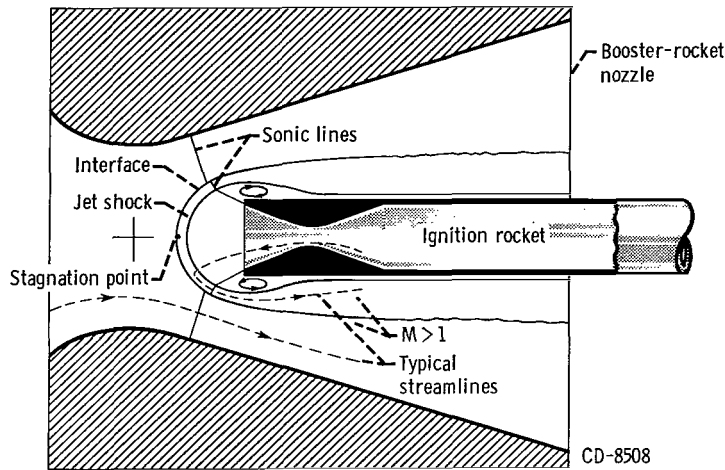


Figure 9. - Ignition-jet-flow boundaries constructed from nozzle Mach number distributions. Ignition-rocket total pressure, 79 pounds per square inch absolute. Ignition-rocket model 5.



(a) Sonic flow in booster throat; effective throat area ratio $\epsilon_e = 1$.



(b) Subsonic flow in booster throat; effective throat area ratio $\epsilon_e < 1$.

Figure 10. - Typical flow patterns in booster nozzle due to ignition-rocket interference when igniter flow does not penetrate booster nozzle throat.

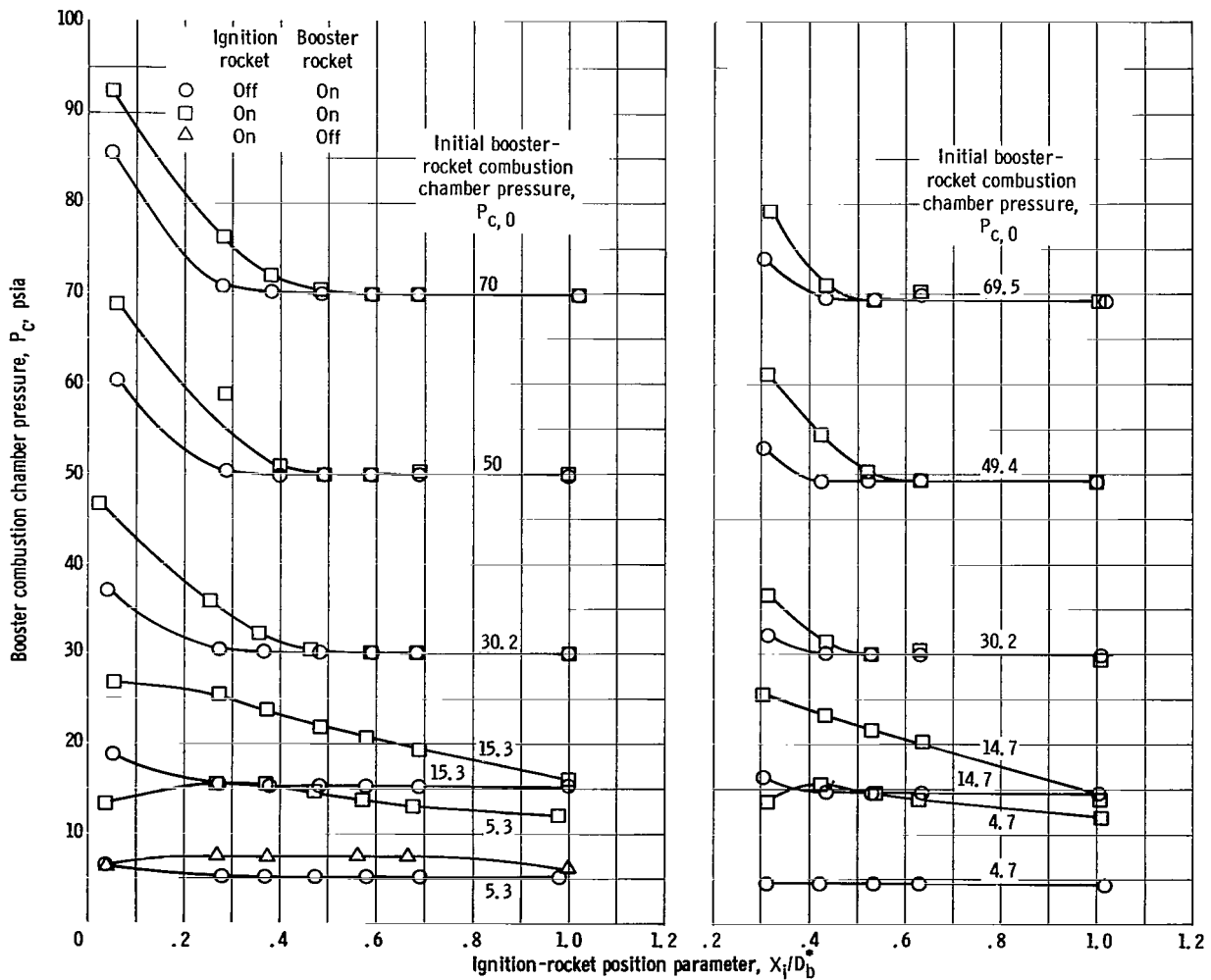
those observed in opposed jet-flow studies, such as reference 2. The initial supersonic flow of the igniter jet terminates in a spherically shaped shock wave. A stagnation point occurs in the subsonic flow field between the bow wave and the jet shock. The subsonic flow expands around the jet shock to supersonic velocity in the exhaust nozzle. Figure 10(a) shows typical streamlines for both the exhaust nozzle flow and the igniter flow.

The case where the ignition-rocket exhaust jet causes an increase in the booster chamber pressure is illustrated in figure 10(b). In this case, the annular area between the nozzle wall and the igniter-jet interface is less than the booster-nozzle throat area,

and the booster chamber pressure must increase to pass the weight flow. The flow at the booster nozzle throat is, therefore, subsonic. The booster chamber pressure will be directly affected, then, by any factor that changes the igniter-jet interface, such as igniter position, weight flow, total pressure, and physical size. When these parameters are changed to alleviate the effective throat area, the flow pattern will revert from the case shown in figure 10(b) to that shown in 10(a).

Basic Data

The variation of the steady-state booster combustion chamber pressure P_c with the ignition-rocket position parameter X_i/D_b^* is shown in figure 11. The data are shown for



(a) Ignition-rocket model 1; ignition-rocket total pressure, 92 pounds per square inch absolute.

(b) Ignition-rocket model 2; ignition-rocket total pressure, 114 pounds per square inch absolute.

Figure 11. - Effect of ignition-rocket position on booster-rocket chamber pressure.

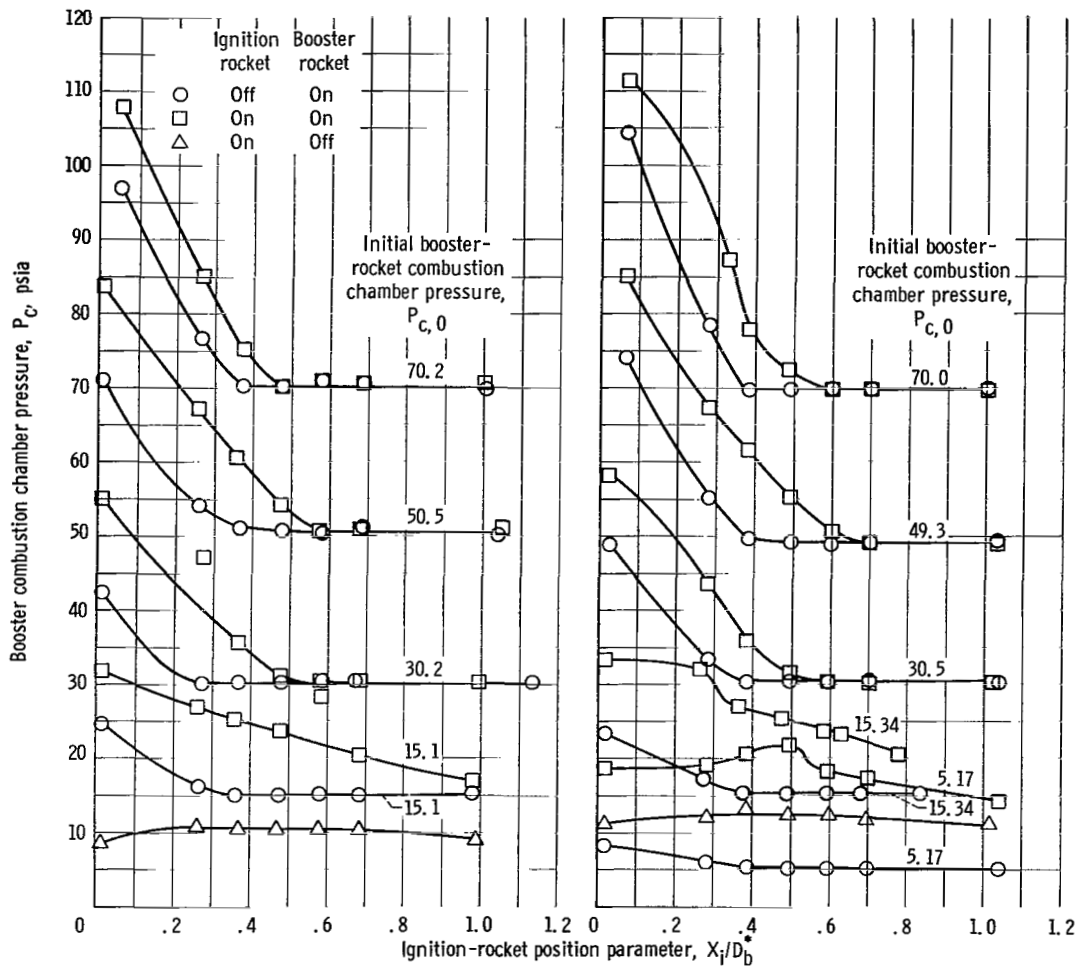
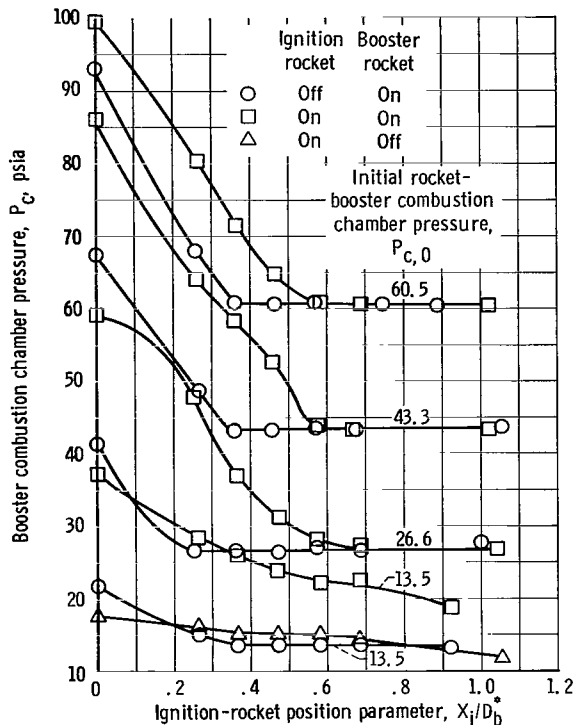


Figure 11. - Continued.

various initial settings of the booster-rocket chamber pressure $P_{c,0}$ set with the ignition rocket withdrawn from the booster nozzle and its jet off. Because of the sonic flow through the simulated grain, the booster mass flow for a given $P_{c,0}$ setting remained constant regardless of an increase in P_c resulting from ignition-rocket interference. Data are also presented for the case where only the ignition jet is on. The latter condition simulates the effect of the ignition jet firing into the booster grain before booster grain ignition.

From consideration of the combustion-chamber overpressurization problem, the data at high $P_{c,0}$ settings are of primary interest. For all the ignition-rocket models tested, the data indicated that, for high chamber pressures, there was no effect of the ignition rocket on the booster chamber pressure at sufficiently high values of X_i/D_b^* . For this condition, the flow phenomenon in the nozzle is of the type shown in figure 10(a).



(e) Ignition-rocket model 5; ignition-rocket total pressure, 79 pounds per square inch absolute.

Figure 11. - Concluded.

As the ignition rocket was moved toward the nozzle throat past a critical value of X_1/D_b^* , for example, X_1/D_b^* of 0.50 for model 1 at $P_{c,0}$ equal to 50 pounds per square inch absolute, the booster chamber pressure began to increase rapidly. At this point, the nozzle flow phenomenon changed to the type illustrated in figure 10(b). The booster-nozzle Mach number variations (fig. 6, p. 7) correlated with these results. At high $P_{c,0}$ settings, the nozzle throat (station A) remained sonic until the ignition rocket was located upstream of X_1/D_b^* of 0.5. For sonic flow at the nozzle throat, as in the case of figure 10(a), the approach to a nozzle pressure tap of the igniter bow wave impingement point is indicated by a decrease in the nozzle Mach number from the design value. This occurred for the pressure tap at station B ($X/D_b^* = 0.5$) for the high $P_{c,0}$ settings when the ignition rocket was at a value of X_1/D_b^* of 0.68.

In addition to determining overpressurization of the combustion chamber, the data are of interest in studying the effectiveness of the aft-end ignition rocket as an ignition system. For rapid and complete ignition of the booster grain, it is desirable for the ignition-rocket jet to have good penetration of the grain port and to raise the pressure in the grain to a level so that the ignition will proceed rapidly. An indication of the effectiveness of the ignition rocket concerning the latter requirement can be obtained from the data where only the ignition jet was on. The maximum chamber pressure in the booster varied from 8 to 22 percent of the ignition-rocket total pressure, depending on the ignition-rocket geometry. The effects of ignition-rocket position appeared to be relatively small for this case.

The effect on the booster-rocket chamber pressure due to the ignition rocket is shown in nondimensional form in figure 12. The ratio of the incremental chamber-pressure increase ΔP_c to the initial combustion-chamber pressure $P_{c,0}$ is shown as a function of the ratio of the ignition-rocket total pressure P_i to the booster-rocket initial pressure $P_{c,0}$. Curves are presented for selected positions of the ignition rocket in the booster nozzle as defined by X_1/D_b^* .

It is evident from figure 12 that both the igniter position and the igniter-to-booster pressure ratio have a large effect on the degree of interference. The igniter-to-booster

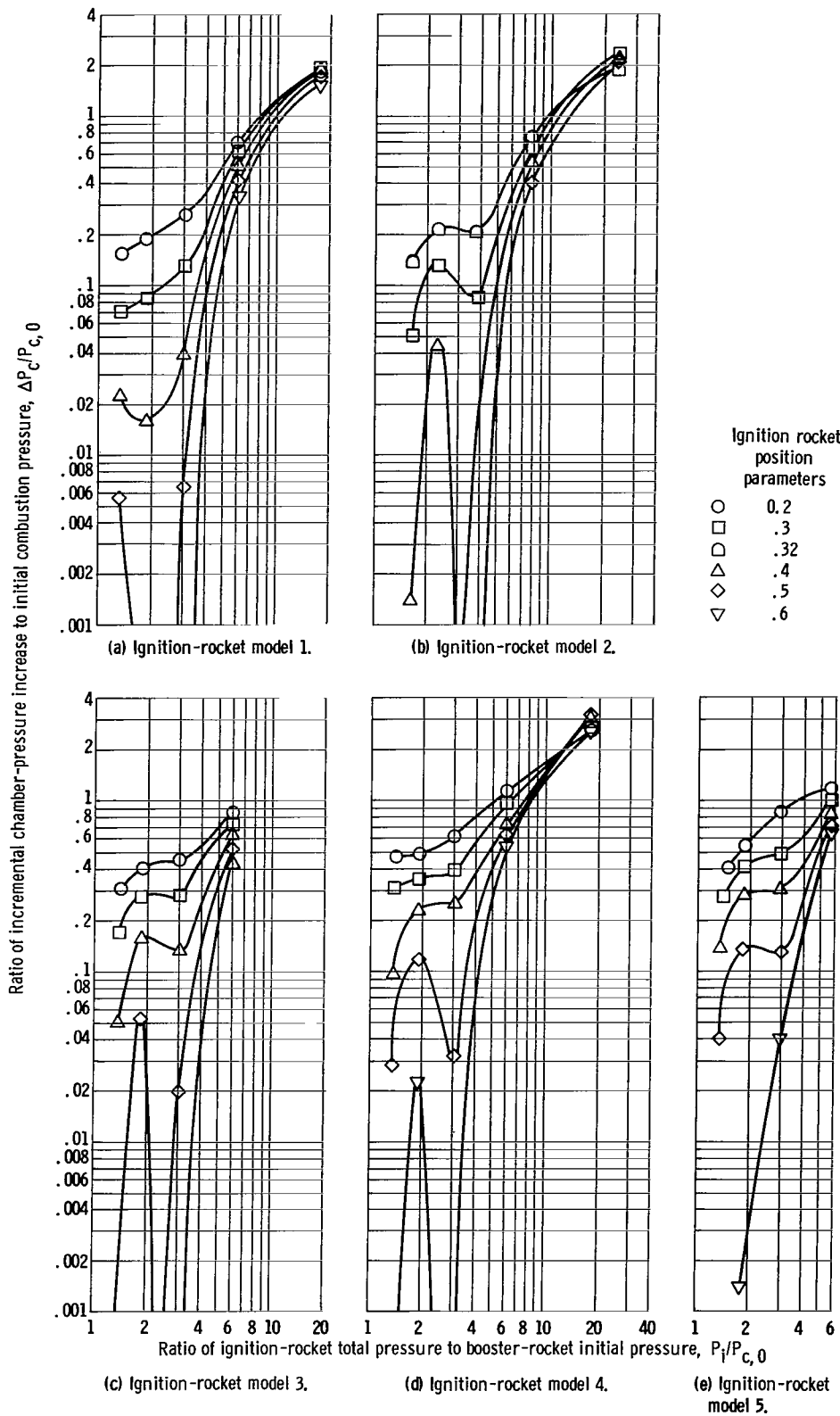


Figure 12. - Effect of ignition-rocket position and pressure ratio on booster-rocket chamber pressure.

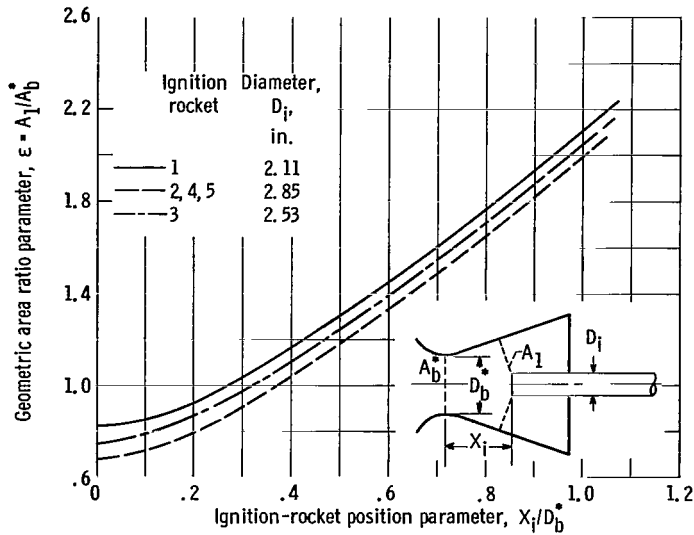


Figure 13. - Effect of ignition-rocket position on area ratio parameter.

pressure ratio for a large booster such as the 260-inch solid rocket varies from about 67 at ignition to about 1.67 at full booster chamber pressure. The curves in figure 12 indicate that, in general, the interference effects decrease rapidly with decreasing pressure ratio. However, at low values of P_i/P_c , this trend suddenly decreased and, in some cases, reversed at a pressure ratio of about 3. The variation of the interference effect with igniter-to-booster pressure ratio can, in general, be correlated with the flow models. At high pressure ratios, the normal shock

pressure recovery of the expanded ignition-rocket jet is considerably higher than the booster chamber pressure, and a large pressure increase occurs in the booster combustion chamber. As the booster chamber pressure is increased to a higher value, the supersonic expansion of the ignition jet is limited so that its normal shock pressure recovery is equal to the booster chamber pressure. For this condition, the relative interference effect is lower and results from a reduced sonic flow area for the booster exhaust gases. The flow phenomenon is similar to that shown in figure 10(b) (p. 12), where the booster exhaust flow passes through the annular flow area outlined by the interface of the reversed ignition jet flow and the nozzle wall. With further increases in the booster chamber pressure, the expanded ignition-jet flow and the spherical shock wave are diminished to the point where they occur at the ignition-rocket nozzle exit or within it. At this point, the normal shock total-pressure loss of the ignition jet becomes small with a correspondingly small variation of its external sonic flow area. The interference effect, therefore, exhibits a small variation at low igniter-to-booster pressure ratios.

At pressure ratios between 1 and 2, which correspond to the range where the booster rocket is at its design chamber pressure, the interference is greatly affected by the ignition rocket position. This result also reflects the fact that the igniter blockage effect tends to become a constant at low pressure ratios and, therefore, the variation of the interference effect with igniter position would be similar to the ϵ variation with igniter position shown in figure 13. The interference effect at low pressure ratios would therefore be expected to be sensitive to igniter diameter. The results for models 3 and 4, which were similar except for the greater diameter of model 4, indicated substantially higher interference values for model 4 (figs. 12(c) and (d)). For all the igniter models

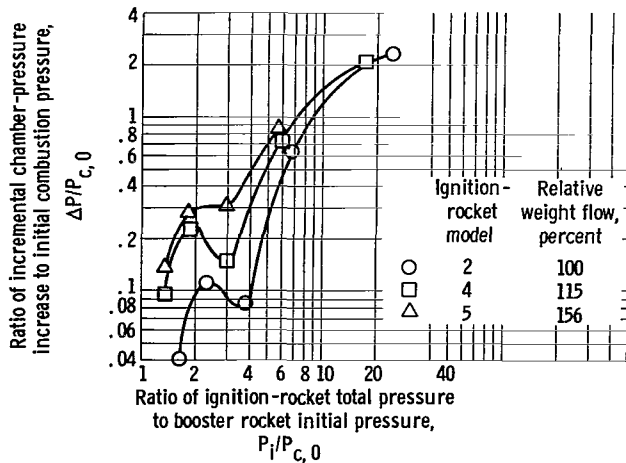


Figure 14. - Effect of ignition-rocket weight flow on booster-rocket chamber pressure. Ignition-rocket position parameter, 0.4.

tested, it can be seen that, for pressure ratios up to 2, the interference was negligible when the ignition rocket was 0.6 throat diameter downstream of the booster throat.

At high pressure ratios, which correspond to the initial booster-ignition phase, the effects of igniter position were relatively small. It can be deduced that, at high pressure ratios, the booster chamber pressure would be directly proportional to the ignition-rocket total pressure. The trends in the data at high pressure ratios also indicate this.

Effect of Igniter Mass Flow

The effect of ignition-rocket mass flow on the variation of the ignition-rocket interference with pressure ratio is shown in figure 14 for ignition-rocket models 2, 4, and 5 at a position equal to 0.4 throat diameter from the booster throat. The relative igniter mass flows of the models with model 2 as a standard were 115 percent for model 4 and 156 percent for model 5. The relative igniter mass flows are determined by the ratios of the product of the igniter throat area and total pressure. The interference effect increases significantly in the critical low-pressure-ratio range with increasing igniter weight flow. These results imply that, in the actual case, it would be advantageous to use the lowest mass-flow ignition rocket that would satisfactorily ignite the booster.

Effective Area Ratio

The interference effects of the ignition rocket discussed in the previous sections can also be interpreted in terms of an effective booster-nozzle-throat area. The booster weight flow at each $P_{c,0}$ setting remained constant because of the choked flow through the simulated grain port. An effective nozzle-area ratio ϵ_e was computed from the relation:

$$\epsilon_e = \frac{A_e^*}{A_b^*} = \frac{P_{c,0}}{P_c}$$

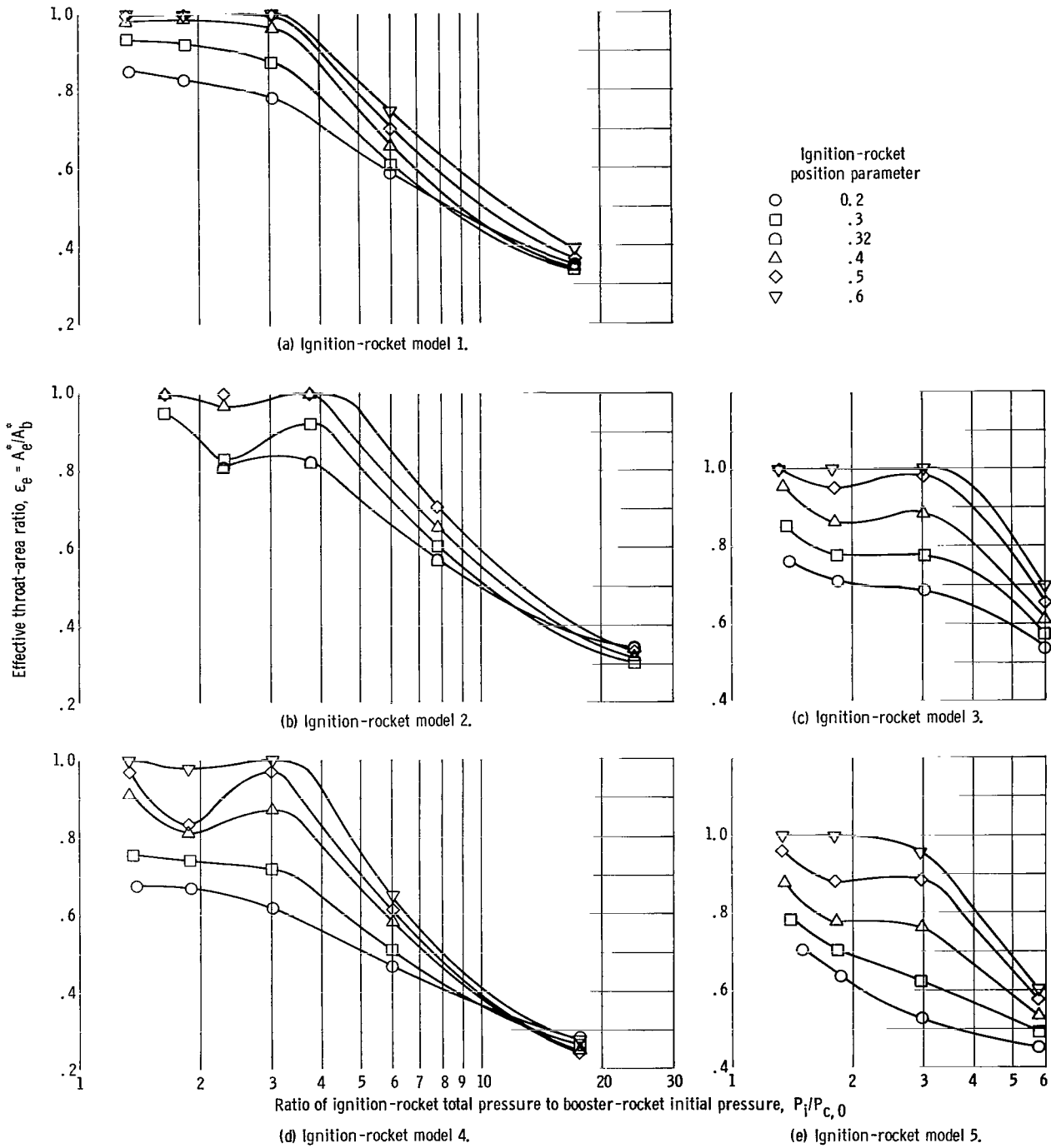


Figure 15. - Effect of igniter-rocket position and igniter-to-booster pressure ratio on effective booster-nozzle throat area.

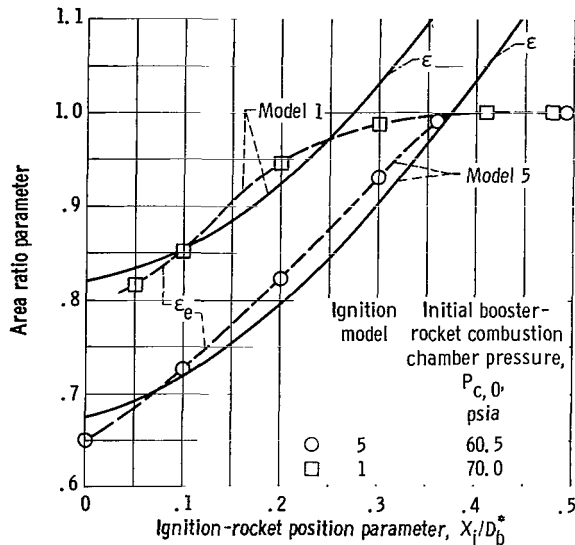


Figure 16. - Comparison of blockage parameter with experimental results. Ignition jet off.

experimental values are compared with the geometric area ratio parameter ϵ . The actual values of ϵ at X_i/D_b^* near zero are less than the geometric values as would be expected because of boundary-layer displacement and vena-contracta effects due to flow about the sharp-edged ignition-rocket model. The data points showing effective values of ϵ greater than the geometric value are the result of experimental inaccuracy.

CONCLUSIONS

The following conclusions are based on the results of a small-scale investigation using compressed-air models to determine the interference effects of an igniter rocket on the chamber pressure of a large, solid rocket.

1. Significant booster-rocket overpressures due to igniter-rocket interference can occur.
2. The interference effect varied with the position of the igniter, the igniter-to-booster pressure ratio, the igniter diameter, and the igniter mass flow.
3. At low igniter-to-booster pressure ratios, which correspond to the booster on-design condition, the effect of igniter position was large with overpressures up to 60 per cent depending on igniter-rocket geometry occurring at an igniter position 0.2 throat diameter downstream of the throat, whereas at igniter positions 0.6 throat diameter downstream, the interference was negligible.

Figure 15 shows ϵ_e as a function of the igniter-to-booster pressure ratio for various values of X_i/D_b^* .

The variation of ϵ_e with igniter-to-booster pressure ratio can be used in the computation of the booster chamber pressure with time, if the relation for the grain-burning rate is also known. However, to apply the values of ϵ_e from figure 15, it is necessary to account for the effects of igniter-to-booster throat-area ratio, if it is different from those presented, and for the external diameter of the igniter rocket.

The effective throat-area ratio for the condition where the igniter rocket is off is shown in figure 16 for models 1 and 5. The

4. At relatively high pressure ratios, which correspond to the initial ignition phase, the booster chamber pressure was a function mainly of the ignition-rocket total pressure, and the effects of igniter position were small.

5. Increasing the igniter weight flow increased the interference effect proportionally.

Lewis Research Center,
National Aeronautics and Space Administration,
Cleveland, Ohio, April 13, 1966.

REFERENCES

1. Niessen, Walter R.: Solid Propellant Rocket Ignition Test and Evaluation (Sprite) Program. AFRPL-TR-65-23, Air Force Rocket Propulsion Laboratory, January, 1965. (Available from DDC as AD-461377.)
2. Hayman, Lovick O., Jr.; and McDearmon, Russell W.: Jet Effects on Cylindrical Afterbodies Housing Sonic and Supersonic Nozzles which Exhaust Against a Supersonic Stream at Angles of Attack from 90° to 180° . NASA TN D-1016, 1962.

"The aeronautical and space activities of the United States shall be conducted so as to contribute . . . to the expansion of human knowledge of phenomena in the atmosphere and space. The Administration shall provide for the widest practicable and appropriate dissemination of information concerning its activities and the results thereof."

—NATIONAL AERONAUTICS AND SPACE ACT OF 1958

NASA SCIENTIFIC AND TECHNICAL PUBLICATIONS

TECHNICAL REPORTS: Scientific and technical information considered important, complete, and a lasting contribution to existing knowledge.

TECHNICAL NOTES: Information less broad in scope but nevertheless of importance as a contribution to existing knowledge.

TECHNICAL MEMORANDUMS: Information receiving limited distribution because of preliminary data, security classification, or other reasons.

CONTRACTOR REPORTS: Technical information generated in connection with a NASA contract or grant and released under NASA auspices.

TECHNICAL TRANSLATIONS: Information published in a foreign language considered to merit NASA distribution in English.

TECHNICAL REPRINTS: Information derived from NASA activities and initially published in the form of journal articles.

SPECIAL PUBLICATIONS: Information derived from or of value to NASA activities but not necessarily reporting the results of individual NASA-programmed scientific efforts. Publications include conference proceedings, monographs, data compilations, handbooks, sourcebooks, and special bibliographies.

Details on the availability of these publications may be obtained from:

SCIENTIFIC AND TECHNICAL INFORMATION DIVISION
NATIONAL AERONAUTICS AND SPACE ADMINISTRATION

Washington, D.C. 20546